Fano-resonant mechanism of terajet formation using graphene-covered high index mesoscale spheres

A.G. PADDUBSKAYA[1,*], A.V. NOVITSKY[2], O.V. MININ[3], AND I.V. MININ[3]

[1] Institute for Nuclear Problems, Belarusian State University, Bobruiskaya Str. 11, Minsk, 220006 Belarus
[2] Belarusian State University, Nezavisimosti Ave. 4, Minsk, 220030 Belarus
[3] National Research Tomsk Polytechnic University, Lenina Ave. 30, Tomsk, 634050 Russia
[*] paddubskaya@gmail.com

Compiled July 15, 2024

Photonic jet in terahertz (THz) frequency range (terajet) plays important role in modern THz scanning systems to achieve a superresolution beyond the diffraction limit. Based on analytical simulations, we introduce synergetic effect of a mesoscale dielectric sphere and graphene to improve focusing properties of the particle. We show that a graphene-covered dielectric sphere is able to enhance the field behind it, if refractive index is high. This conflicts with a generally accepted statement that a jet is generated only for low-index dielectrics with $n < 2$. We demonstrate tunability of the terajet characteristics with respect to the graphene Fermi energy and discover a Fano resonance causing the field increase. This design leverages the tuning properties of the graphene allowing dynamic control over the power and size of the generated terajet in real-time. With high-index materials we get the opportunity for integration of the terajet-assisted imaging with semiconductor technology.

http://dx.doi.org/10.1364/ao.XX.XXXXXX

In 2004, Chen et al. [1] numerically demonstrated that lossless spherical or elliptical microparticles are able to generate extremely narrow-focused, high-intensity electromagnetic beam with sub-wavelength lateral dimensions, known as photonic nanojet (PNJ). This work showed that it is possible to significantly exceed the classical diffraction limit, opening new avenues for improving the resolution of existing technologies [2–5]. Today, the concept of PNJ has found a wide range of applications in modern optics, including high-resolution imaging [6, 7], Raman and two-photon fluorescence enhancement spectroscopy [8], nanoparticle detection and manipulation [9, 10], low-loss coupled resonator optical waveguiding and nanolithography [11, 12].

Recently, a terajet as a terahertz (THz) analog of the photonic jet [3], has been proposed as a simple and effective method to overcome the diffraction limit in the THz frequency range (0.1-10 THz), where the wavelength is much longer compared to that of visible light [13, 14]. In particular, sub-wavelength spatial resolution below the Rayleigh limit ($\sim 0.33\lambda$) was experimentally demonstrated using a Teflon sphere in Refs. [15]. The potential of such a sphere-coupled THz system for *in situ* analysis of thin and almost transparent dielectric films or nonconductive biomaterials has been analyzed in our previous work [16]. Geometry of the terajet generator can be diverse. In Ref. [17], the mesoscale dielectric cube was first proposed as a focusing particle to enhance the resolution of the THz imaging system.

Several approaches have been proposed to control and manipulate the intensity, shape, and dimensions of the terajet. However, in most published works, the key parameters of the generated terajet, such as the maximum electric field enhancement, effective length, and focusing position, are predominantly determined by the invariable dielectric material properties, making it challenging to adjust these parameters in real-time within a single design of focusing particle [18, 19]. These limitations significantly restrict the potential of the terajet-assisted approach.

Graphene, known for its extraordinary properties, is considered as one of the most promising materials for THz applications [20–22]. Its sheet conductivity can be efficiently tuned across a broad frequency range by applying an external electromagnetic field or incident optical excitation [23, 24]. This tunability makes graphene attractive for practical designing integrated devices operating in the microwave to THz frequency range. Despite its negligible thickness, graphene is efficiently used for electromagnetic wave shielding and absorption [25–27]. Due to graphene's flexibility, it can be configured into complex structures with fascinating properties, whose spectral response can be successfully governed [28]. For example, the spectral tunability of the resonance peak of graphene-coated cylinders was demonstrated in Refs. [19, 29].

In this work, we numerically demonstrate the advantages of using a graphene-coated dielectric sphere to dynamically control and manipulate parameters of terajets. Our simulation results reveal that graphene facilitates formation of the terajet with high reflective index dielectrics prohibited for nanojet generation so far [3]. This expands the possibilities for widespread use of the near-field THz imaging.

We calculate the scattered field by adopting the operator scattering approach developed for anisotropic multilayer rotationally symmetric spheres (see, [30–32]). Consider a spherical particle with a diameter d and refractive index n, coated with a graphene layer. The whole structure is assumed to be centered

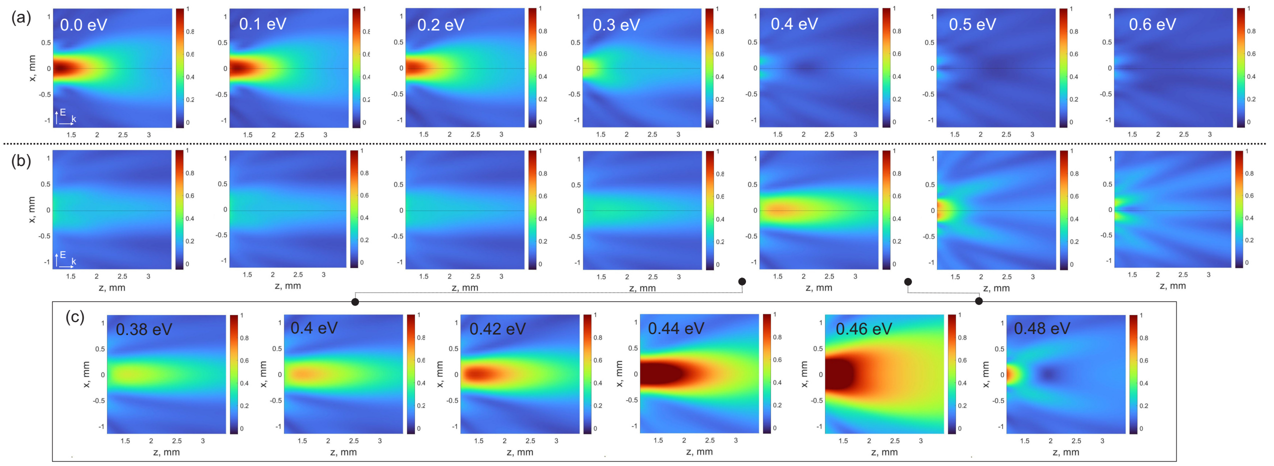

Fig. 1. Distribution of the electric field amplitude $|E|$ behind the dielectric core/graphene shell structure as a function of the graphene chemical potential E_F and the sphere refractive index: (a) $n = 1.47$ and (b) $n = 3.42$. Incident Gaussian beam of frequency of 0.7 THz is x- polarized. Panel (c) shows the electric field distribution at intermediate values of the Fermi energy in the case $n = 3.42$. All data were normalized by the maximum terajet field amplitude at $n = 1.47$ and $E_F = 0$ eV.

at the origin of the Cartesian coordinate system. Linearly polarized incident light propagates along the z–axis. We calculate the scattering of the electromagnetic THz Gaussian beam in paraxial approximation, which electric field reads

$$\mathbf{E} = \mathbf{e}A\frac{w_0}{{w_0}^2+2iz/k_0}\exp\left(ik_0z-\frac{\rho^2}{{w_0}^2+2iz/k_0}\right). \tag{1}$$

Here, ρ is the polar coordinate in the cross-section of the THz beam, z is the longitudinal coordinate, A represents the field at the point ($\rho = 0, z = 0$), $\mathbf{e}$ is the wave polarization, $k_0 = 2\pi f/c$ is the wave number in vacuum, f is the frequency of incident beam and c is the speed of light in vacuum. Parameter w_0 denotes the waist radius of the Gaussian beam.

According to the operator scattering theory, the electromagnetic field is series expanded with respect to the matrix spherical harmonics $F_{lm}(\theta,\varphi)$, where (r,θ,φ) are spherical coordinates and $l = 0, 1, \ldots$ and $-l \leq m \leq l$ are integer numbers. Using the orthogonality condition for spherical harmonics $F_{lm}(\theta,\varphi)$, we can find the expansion coefficients $\mathbf{E}^{(inc)}_{lm}(r)$ appearing in the series expansion of the incident wave

$$\mathbf{E}^{(inc)}(\mathbf{r}) = \sum_{l=1}^{\infty}\sum_{m=-l}^{l}F_{lm}(\theta,\varphi)\mathbf{E}^{(inc)}_{im}(r). \tag{2}$$

Writing the series for scattered and inner fields in the form similar to Eq. (2), one can express the scattered magnetic field at the interface between the particle and surrounding as [30]

$$\mathbf{H}^{(sc)}_{lm} = -\left[({\Gamma_1}^l - I)\Omega\begin{pmatrix} I\\ \tilde{\Gamma}_1\end{pmatrix}\right]^{-1}\left[({\Gamma_1}^l - I)\Omega\mathbf{W}^{(inc)}_{lm}\right]. \tag{3}$$

Here I is the two-dimensional unit matrix, Γ_1^l is the surface wave impedance matrix at the first inner interface of multilayer particle (characterizes the core), $\tilde{\Gamma}^l$ is the surface wave impedance matrix at the outer interface (characterizes the ambient medium), Ω is the evolution operator of the multilayer particle (characterizes the cladding layers). Expansion coefficients for the incident field at the outer interface of the spherical particle are given by $\mathbf{W}^{(inc)}_{lm}$. They include the expansion coefficients for electric $\mathbf{E}^{(inc)}_{t,lm}$ and magnetic $\mathbf{H}^{(inc)}_{t,lm}$ tangential fields as

$$\mathbf{W}^{(inc)}_{lm} = \begin{pmatrix} \mathbf{H}^{(inc)}_{t,lm}\\ \mathbf{E}^{(inc)}_{t,lm}\end{pmatrix}. \tag{4}$$

Evolution operator Ω in Eq. (3) representing a four-dimensional matrix is a product of evolution operators of individual cladding layers. A graphene cover can be incorporated into this scheme, being considered as an infinitely thin layer characterized by surface conductivity σ_s. The graphene evolution operator reads

$$\Omega_g = \begin{pmatrix} I & I\sigma_s\\ 0 & I\end{pmatrix}. \tag{5}$$

In the absence of disorder, the surface conductivity of graphene σ_s in the THz frequency range is predominantly determined by intraband transitions and can be accurately described by the Drude model as follows [33]

$$\sigma_s = \frac{\sigma_0}{1+i\omega\tau}. \tag{6}$$

where $\sigma_0 = e^2E_F\tau/\pi\hbar^2$ is the static conductivity of graphene; $\tau = \mu\hbar\sqrt{n_s\pi}/ev_F$ and $n_s = E_F^2/\pi\hbar^2v_F^2$ are the carrier relaxation time and mobility, respectively; E_F is the Fermi energy or the chemical potential ($|E_F| \gg k_BT$ in THz frequency range), which can be controlled by either an applied electrostatic bias, or chemical doping, or strain engineering; $v_F = 10^6$ m/s is the Fermi velocity; k_B and $\hbar$ are the Boltzmann's and reduced Planck's constant, respectively. Carrier relaxation time of graphene τ equals 7×10^{-13} s.

Since we have only a graphene sheet as a cover of the dielectric core, the evolution operator is $\Omega = \Omega_g$. With the known scattering amplitudes $\mathbf{H}^{(sc)}_{lm}$ provided by Eq.(3), one can calculate the scattered and total fields both inside and outside the particle.

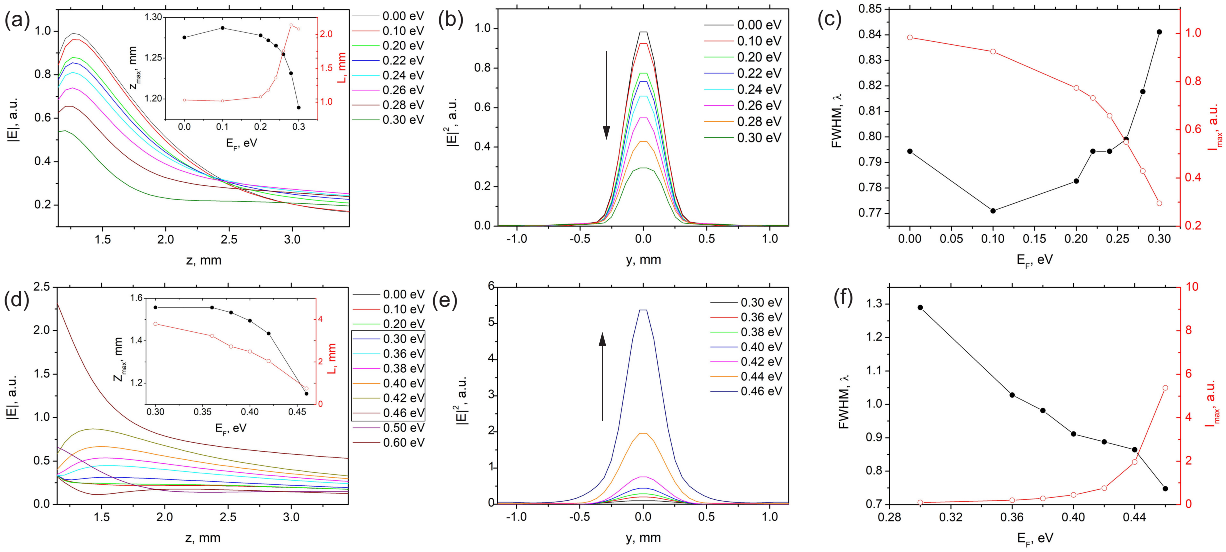

Fig. 2. (a, d) Electric field amplitude profiles along the z-axis and (b, e) transverse profile of terajet intensity $|E|^2$ at the focal point calculated for different E_F of the dielectric core/graphene shell structure. The insets in the upper right corner of panels (a, d) illustrate the correlation between focus position z_{max} and terajet length L. (c, f) FWHM and intensity at the terajet focal point I_{max} as a function of E_F. The upper row (a - c) corresponds to $n = 1.47$ and the lower row (d - f) corresponds to $n = 3.42$. All data were normalized by the maximum terajet field amplitude at $n = 1.47$ and $E_F = 0$ eV.

Figure 1 shows the field distribution $|E|$ near the surface of the dielectric sphere illuminated by THz radiation at the frequency 0.7 THz. We performed the numerical calculations for a sphere with a diameter of 2.3 mm and refractive indices 1.47 (Teflon) and 3.42 (silicon). The waist radius of the focused Gaussian beam is set to $w_0 = 1.15$ mm and the refractive index of the surrounding environment is assumed to be 1. It should be noted that the beam and particle parameters were chosen in accordance with the experimental configuration in [16]. For clarity, we consider only the case of the x-polarized incident beam, although similar results are observed also for y-polarized Gaussian beams.

According to Eq. 6, when the graphene Fermi energy $E_F = 0$ (left column in Fig. 1), the graphene conductivity equals zero, implying scattering of the electromagnetic wave by the uncovered dielectric sphere. Notable, for the refractive index $n = 1.47$, a narrow high-intensity beam (terajet) is observed on the shadow side of the dielectric sphere. On the other hand, for refractive indices $n > 2$ as in Fig. 1)b, the incident light is focused inside the spherical particle, which can be clearly explained using the spherical lens formula (see, for example, [3]).

It should be noted that almost all polymers have a refractive index in the range of $1 < n < 2$ at THz frequencies, making them suitable for imaging applications. It is not the case for the silicon possessing refractive index around $n = 3.4$ (undoped silicon has the dielectric permittivity 11 to 13 and loss tangent $\sim 10^{-4} - 10^{-5}$ [34]), in spite of it is a widespread material in modern device fabrication technology, including CMOS (complementary metal-oxide-semiconductor) fabrication platform.

As illustrated in Fig. 1, incorporation of the graphene cover layer ($E_F \neq 0$) significantly changes electromagnetic field distribution near the surface of the dielectric sphere. The calculated electric field amplitude profiles along the z-axis for such a core-shell structure with refractive indices $n = 1.47$ and $n = 3.42$ are presented in Figs. 2a and 2d, respectively. The insets in Figs. 2a and 2b show the correlation between the focus position and jet length L defined as the distance along the z-axis at which the field amplitude drops to $1/e$ of its maximum value, where $e = 2.718\ldots$.

For $n = 1.47$, it is observed in Figs. 1a and 2a that the jet focus position shifts toward the sphere as the graphene doping level E_F increases. At $E_F = 0.3$ eV the length L increases up to two times compared to the length without graphene layer. Figure 2b shows the transverse profile of the terajet intensity $I \sim |E|^2$ calculated at the terajet focal point as a function of E_F. The corresponding values of the full width at half maximum (FWHM) and the maximum intensity at the terajet focal points (I_{max}) are presented in Fig. 2c. According to these plots, it can be concluded that for $n = 1.47$ the FWHM increases as E_F increases (from 0.79λ for $E_F = 0$ eV to 0.84λ for $E_F = 0.3$eV), while I_{max} decreases with increasing E_F.

To qualitatively understand the terajet formation, detailed simulations of the field distribution both inside and outside the structure are carried out (see Fig. 3). Suppression of the terajet intensity for the structure with core refractive index $n < 2$ observed in Fig. 3c can be qualitatively explained by increasing absorption in the graphene shell as E_F rises. Thus, by varying the graphene Fermi level, it is possible to control the power characteristics and spatial dimensions of the generated terajet. Our results well align with theoretical predictions published in [35], where graphene-based gradient reflective index structures were considered as tunable Luneberg lenses.

The contrasting behavior is observed for the core-shell structure with high core refractive index $n = 3.42$. As shown in Fig. 1b, formation of a terajet behind the dielectric sphere occurs when 0.36 eV $< E_F <$ 0.46 eV. The essential thing is that as E_F increases within this range, the FWHM of the formed terajet decreases, while I_{max} simultaneously increases (see Fig. 2f), reaching values up to 5 times larger at $E_F = 0.46$ eV compared to the bare dielectric sphere with $n = 1.47$ (see Fig. 2e).

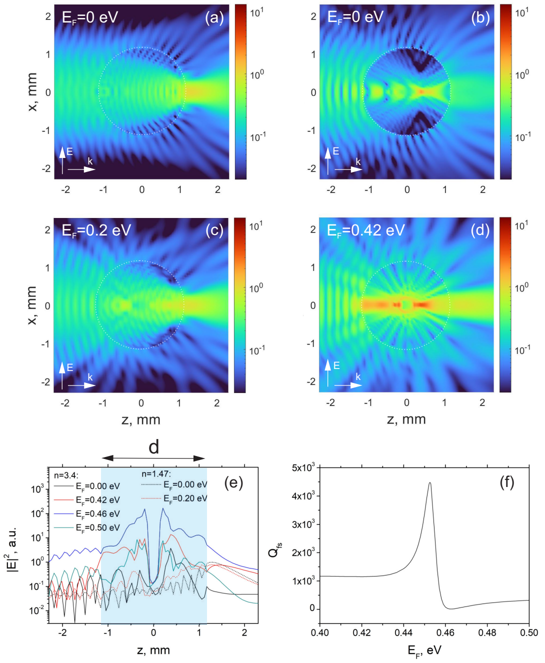

Fig. 3. Distribution of the electric field amplitude $|E|$ both outside and inside the dielectric core/graphene shell structure illuminated by the focused Gaussian beam: (a, c) $n = 1.47$ and (b, d) $n = 3.42$. (e) The electromagnetic field intensity $|E|^2$ profiles along the z-axis at $x = 0$. (f) Efficiency of forward scattering calculated for the dielectric core/graphene shell spherical structure with $n = 3.42$ as a function of E_F.

As mentioned earlier and illustrated in Fig. 3b, the incident light is predominantly focused inside the dielectric particle for $E_F = 0$ and $n > 2$. With an increase of the doping level, a significant enhancement of the electromagnetic field inside the dielectric sphere is observed (see the blue line in Fig. 3e). To clarify the physical mechanism behind this field enhancement and the resulting terajet formation on the shadow side of the dielectric particle with high refractive index, the forward scattering efficiency Q_{fs} has been numerically calculated (see the supplementary materials for details). The scattering efficiency as a function of E_F demonstrated in Fig. 3f exhibits a high-quality asymmetric resonance (Fano resonance) at E_F = 0.454 eV. Based on the multipole decomposition analysis within the Mie theory, we reveal that the interference between a narrow magnetic mode with Mie coefficient b_8 and broad modes with Mie coefficients $b_{1,2}$ causes this resonance. Thus, the terajet generated by a graphene-coated spherical particle with $n > 2$ is attributed to the Fano resonance excited in such a structure.

In conclusion, using the operator scattering theory we have calculated electromagnetic near-fields for a dielectric sphere with an infinitesimally thin conductive graphene cover. We have discovered a terajet generated by the graphene-covered dielectric sphere illuminated by a Gaussian beam and analyzed its key characteristics as focal point position, peak intensity, and FWHM. We have drawn an important conclusion that manipulating graphene Fermi energy E_F is an indispensable tool for terajet generation across a wide range of materials, including those with a refractive index $n > 2$ providing a precise control over the power characteristics and spatial distributions of the terajet. Using the example of silicon spherical bead coated with graphene, we have clearly shown that the asymmetric Fano resonance causes a significant field enhancement behind the particle. It is important to highlight that, to the best of our knowledge, this research explores the use of graphene as a tunable shell for jet generation for the first time. Our results may dramatically affect the development of tunable THz imaging systems and other related applications.

Acknowledgments. This work was supported by the Tomsk Polytechnic University Development Program and by BRFBR project no. F23ME-023. A.V. Novitsky acknowledges the support of the Research Program “Convergence-2025” (project no. 2.1.02.1).

Disclosures. The authors declare no conflicts of interest.

Data Availability Statement. The data that support the findings of this study are available within the article and from the corresponding author upon reasonable request.

Supplemental document. See Supplement 1 for supporting content

REFERENCES

1. Z. Chen, A. Taflove, and V. Backman, Opt. Express **12**, 1214 (2004).
2. G. Wu and M. Hong, Engineering (2024).
3. B. S. Luk’yanchuk, R. Paniagua-Domínguez, I. V. Minin, *et al.*, Opt. Mater. Express **7**, 1820 (2017).
4. R. Chen, J. Lin, P. Jin, *et al.*, Opt. Commun. **456**, 124593 (2020).
5. J. Zhu and L. L. Goddard, Nanoscale Adv. **1**, 4615 (2019).
6. L. Li, W. Guo, Y. Yan, *et al.*, Light. Sci. & Appl. **2**, e104 (2013).
7. Y. Li, C. Qiu, H. Ji, *et al.*, Adv. Opt. Mater. p. 2300172 (2023).
8. H. S. Patel, P. K. Kushwaha, and M. K. Swami, J. Appl. Phys. **123**, 023102 (2018).
9. H. Yang, M. Cornaglia, and M. A. M. Gijs, Nano Lett. **15**, 1730 (2015).
10. H. Wang, X. Wu, and D. Shen, Opt. Lett. **41**, 1652 (2016).
11. J. Kim, K. Cho, I. Kim, *et al.*, Appl. Phys. Express **5**, 025201 (2012).
12. A. Darafsheh, J. Physics: Photonics **3**, 022001 (2021).
13. V. Pacheco-Peña, M. Beruete, I. V. Minin, and O. V. Minin, Opt. Lett. **40**, 245 (2015).
14. I. V. Minin and O. V. Minin, Opt. Quantum Electron. **49**, 326 (2017).
15. Y. Yang, H. Liu, M. Yang, *et al.*, Appl. Phys. Lett. **113**, 031105 (2018).
16. A. G. Paddubskaya, N. I. Valynets, A. V. Novitsky, *et al.*, J. Phys. D: Appl. Phys. **57**, 145104 (2024).
17. H. H. Nguyen Pham, S. Hisatake, O. V. Minin, *et al.*, APL Photonics **2**, 056106 (2017).
18. I. Fanyaev, I. Faniayeu, J. Li, and S. Khakhomov, Results Phys. **52**, 106917 (2023).
19. C. L. Wang, Y. Q. Wang, H. Hu, *et al.*, Opt. Express **27**, 35925 (2019).
20. L. Viti, D. G. Purdie, A. Lombardo, *et al.*, Nano Lett. **20**, 3169 (2020).
21. L. Viti, A. R. Cadore, X. Yang, *et al.*, Nanophotonics **10**, 89 (2021).
22. S. Castilla, B. Terrés, M. Autore, *et al.*, Nano Lett. **19**, 2765 (2019).
23. R. Ivaškevičiūtė-Povilauskienė, A. Paddubskaya, D. Seliuta, *et al.*, J. Appl. Phys. **131**, 033101 (2022).
24. J. Wang, F. Ma, W. Liang, *et al.*, Nanophotonics **6**, 943 (2017).
25. K. Batrakov, P. Kuzhir, S. Maksimenko, *et al.*, Sci. Reports **4**, 7191 (2014).
26. Y. Zhang, Y. Feng, B. Zhu, *et al.*, Opt. Express **22**, 22743 (2014).
27. Y. Xia, W. Gao, and C. Gao, Adv. Funct. Mater. **32**, 2204591 (2022).
28. M. Baah, A. Paddubskaya, A. Novitsky, *et al.*, Carbon **185**, 709 (2021).
29. H. Pashaeiadl, M. Naserpour, and C. J. Zapata-Rodríguez, Optik **159**, 123 (2018).
30. A. Novitsky and L. Barkovsky, PRA **77**, 033849 (2008).
31. A. Novitsky, C.-W. Qiu, and H. Wang, PRL **107**, 203601 (2011).
32. A. Novitsky, A. S. Shalin, and A. V. Lavrinenko, PRA **95**, 053818 (2017).
33. A. Ferreira, J. Viana-Gomes, Y. V. Bludov, *et al.*, PRB **84**, 235410 (2011).
34. E. D. Palik, *Handbook of optical constants of solids*, vol. 3 (Academic press, 1998).
35. F. Moharrami and Z. Atlasbaf, J. Opt. **22**, 025102 (2020).

FULL REFERENCES

1. Z. Chen, A. Taflove, and V. Backman, “Photonic nanojet enhancement of backscattering of light by nanoparticles: a potential novel visible-light ultramicroscopy technique,” Opt. Express **12**, 1214–1220 (2004).
2. G. Wu and M. Hong, “Optical microsphere nano-imaging: Progress and challenges,” Engineering (2024).
3. B. S. Luk’yanchuk, R. Paniagua-Domínguez, I. V. Minin, *et al.*, “Refractive index less than two: photonic nanojets yesterday, today and tomorrow [invited],” Opt. Mater. Express **7**, 1820–1847 (2017).
4. R. Chen, J. Lin, P. Jin, *et al.*, “Photonic nanojet beam shaping by illumination polarization engineering,” Opt. Commun. **456**, 124593 (2020).
5. J. Zhu and L. L. Goddard, “All-dielectric concentration of electromagnetic fields at the nanoscale: the role of photonic nanojets,” Nanoscale Adv. **1**, 4615–4643 (2019).
6. L. Li, W. Guo, Y. Yan, *et al.*, “Label-free super-resolution imaging of adenoviruses by submerged microsphere optical nanoscopy,” Light. Sci. & Appl. **2**, e104–e104 (2013).
7. Y. Li, C. Qiu, H. Ji, *et al.*, “Microsphere-aided super-resolution scanning spectral and photocurrent microscopy for optoelectronic devices,” Adv. Opt. Mater. p. 2300172 (2023).
8. H. S. Patel, P. K. Kushwaha, and M. K. Swami, “Photonic nanojet assisted enhancement of raman signal: Effect of refractive index contrast,” J. Appl. Phys. **123**, 023102 (2018).
9. H. Yang, M. Cornaglia, and M. A. M. Gijs, “Photonic nanojet array for fast detection of single nanoparticles in a flow,” Nano Lett. **15**, 1730–1735 (2015).
10. H. Wang, X. Wu, and D. Shen, “Trapping and manipulating nanoparticles in photonic nanojets,” Opt. Lett. **41**, 1652–1655 (2016).
11. J. Kim, K. Cho, I. Kim, *et al.*, “Fabrication of plasmonic nanodiscs by photonic nanojet lithography,” Appl. Phys. Express **5**, 025201 (2012).
12. A. Darafsheh, “Photonic nanojets and their applications,” J. Physics: Photonics **3**, 022001 (2021).
13. V. Pacheco-Peña, M. Beruete, I. V. Minin, and O. V. Minin, “Multifrequency focusing and wide angular scanning of terajets,” Opt. Lett. **40**, 245–248 (2015).
14. I. V. Minin and O. V. Minin, “Terahertz artificial dielectric cuboid lens on substrate for super-resolution images,” Opt. Quantum Electron. **49**, 326 (2017).
15. Y. Yang, H. Liu, M. Yang, *et al.*, “Dielectric sphere-coupled thz super-resolution imaging,” Appl. Phys. Lett. **113**, 031105 (2018).
16. A. G. Paddubskaya, N. I. Valynets, A. V. Novitsky, *et al.*, “Terajet-assisted time-domain super-resolution imaging,” J. Phys. D: Appl. Phys. **57**, 145104 (2024).
17. H. H. Nguyen Pham, S. Hisatake, O. V. Minin, *et al.*, “Enhancement of spatial resolution of terahertz imaging systems based on terajet generation by dielectric cube,” APL Photonics **2**, 056106 (2017).
18. I. Fanyaev, I. Faniayeu, J. Li, and S. Khakhomov, “Subwavelength imaging amplification via electro-thermally tunable insb-graphene-based hyperlens in terahertz frequency,” Results Phys. **52**, 106917 (2023).
19. C. L. Wang, Y. Q. Wang, H. Hu, *et al.*, “Reconfigurable sensor and nanoantenna by graphene-tuned fano resonance,” Opt. Express **27**, 35925–35934 (2019).
20. L. Viti, D. G. Purdie, A. Lombardo, *et al.*, “Hbn-encapsulated, graphene-based, room-temperature terahertz receivers, with high speed and low noise,” Nano Lett. **20**, 3169–3177 (2020).
21. L. Viti, A. R. Cadore, X. Yang, *et al.*, “Thermoelectric graphene photodetectors with sub-nanosecond response times at terahertz frequencies,” Nanophotonics **10**, 89–98 (2021).
22. S. Castilla, B. Terrés, M. Autore, *et al.*, “Fast and sensitive terahertz detection using an antenna-integrated graphene pn junction,” Nano Lett. **19**, 2765–2773 (2019).
23. R. Ivaškevičiūtė-Povilauskienė, A. Paddubskaya, D. Seliuta, *et al.*, “Advantages of optical modulation in terahertz imaging for study of graphene layers,” J. Appl. Phys. **131**, 033101 (2022).
24. J. Wang, F. Ma, W. Liang, *et al.*, “Optical, photonic and optoelectronic properties of graphene, h-bn and their hybrid materials,” Nanophotonics **6**, 943–976 (2017).
25. K. Batrakov, P. Kuzhir, S. Maksimenko, *et al.*, “Flexible transparent graphene/polymer multilayers for efficient electromagnetic field absorption,” Sci. Reports **4**, 7191 (2014).
26. Y. Zhang, Y. Feng, B. Zhu, *et al.*, “Graphene based tunable metamaterial absorber and polarization modulation in terahertz frequency,” Opt. Express **22**, 22743–22752 (2014).
27. Y. Xia, W. Gao, and C. Gao, “A review on graphene-based electromagnetic functional materials: Electromagnetic wave shielding and absorption,” Adv. Funct. Mater. **32**, 2204591 (2022).
28. M. Baah, A. Paddubskaya, A. Novitsky, *et al.*, “All-graphene perfect broadband thz absorber,” Carbon **185**, 709–716 (2021).
29. H. Pashaeiadl, M. Naserpour, and C. J. Zapata-Rodríguez, “Scattering of electromagnetic waves by a graphene-coated thin cylinder of left-handed metamaterial,” Optik **159**, 123–132 (2018).
30. A. Novitsky and L. Barkovsky, “Matrix approach for light scattering from a multilayered rotationally symmetric bianisotropic sphere,” PRA **77**, 033849 (2008).
31. A. Novitsky, C.-W. Qiu, and H. Wang, “Single gradientless light beam drags particles as tractor beams,” PRL **107**, 203601 (2011).
32. A. Novitsky, A. S. Shalin, and A. V. Lavrinenko, “Spherically symmetric inhomogeneous bianisotropic media: Wave propagation and light scattering,” PRA **95**, 053818 (2017).
33. A. Ferreira, J. Viana-Gomes, Y. V. Bludov, *et al.*, “Faraday effect in graphene enclosed in an optical cavity and the equation of motion method for the study of magneto-optical transport in solids,” PRB **84**, 235410 (2011).
34. E. D. Palik, *Handbook of optical constants of solids*, vol. 3 (Academic press, 1998).
35. F. Moharrami and Z. Atlasbaf, “Tunable grin lensing based on graphene-dielectric multilayer metamaterials,” J. Opt. **22**, 025102 (2020).